# A Highly Stabilized Low-Noise GaAs FET Integrated Oscillator with a Dielectric Resonator in the *C* Band

HIROYUKI ABE, YOICHIRO TAKAYAMA, MEMBER, IEEE, ASAMITSU HIGASHISAKA, AND HIDEO TAKAMIZAWA

*Abstract*—**A GaAs FET integrated oscillator stabilized with a $BaO$–$TiO_2$ system ceramic dielectric resonator provides a high-frequency-stabilized low-noise compact microwave power source. The newly developed ceramic has an expansion coefficient and dielectric constant temperature coefficient that offset each other and result in a small resonant frequency temperature coefficient. A stabilized oscillator output of 100 mW with a 17-percent efficiency and a frequency temperature coefficient as low as 2.3 ppm/°C are obtained at 6 GHz. FM noise level is reduced more the 30 dB by the stabilization. The dynamic properties of the oscillator and resonator are precisely measured to determine equivalent circuit representations. A large-signal design theory based on these equivalent circuit representations is presented to realize the optimal coupling condition between the oscillator and stabilizing resonator. The stabilized oscillator performance is sufficient for application to microwave communications systems.**

## I. Introduction

GALLIUM ARSENIDE field effect transistor oscillators with an external feedback network have exhibited high-power high-efficiency microwave performance [1]. GaAs FET oscillators have been reported in use as frequency-stabilized sources and swept frequency sources [2], [3]. To use a GaAs FET oscillator as a power source in microwave communications systems, high-frequency stability and low-noise characteristics are essential.

D. S. James *et al.* stabilized GaAs FET oscillators with invar and titanium silicate resonant cavities, used as band pass filters [2]. In the *C* band the resonant cavity is relatively large. Furthermore, difficult problems lie in coupling a resonant cavity directly to an FET oscillator fabricated with microstriplines.

A highly stabilized low-noise GaAs FET oscillator is realized in the *C* band by the use of a dielectric resonator. This dielectric resonator is placed at the oscillator drain output terminal as a band rejection filter. This dielectric resonator with high resonant frequency stability is made of a newly developed $BaO$–$TiO_2$ system ceramic. This material has an expansion coefficient and dielectric constant temperature coefficient that offset each other and result in a small resonant frequency temperature coefficient. Improved stabilization can be effected with a low-loss dielectric resonator because of the resonator's small size and easy coupling with the oscillator [4].

Manuscript received March 30, 1977, revised August 9, 1977.

The authors are with the Central Research Laboratories, Nippon Electric Co., Ltd., Miyazaki, Takatsu-ku, Kawasaki 213, Japan.

The oscillator load characteristics and reflection characteristics of the resonator magnetically coupled to a 50-Ω microstripline are precisely measured, and the equivalent circuit representations are determined. A large-signal design theory, based on these equivalent circuit representations, is presented to realize optimal coupling between the oscillator and stabilizing resonant circuit.

## II. GaAs FET Oscillator Performance Before Stabilization

In this study, GaAs FET chips, developed for medium power applications by A. Higashisaka *et al.* in the NEC Central Research Laboratories, were used [5]. The gate length is 1.5 μm and the total gate width is 2500 μm. When this FET chip is used as an amplifier under common-source class A operating conditions, the saturated power level is 600 mW with a 5-dB gain (power added efficiency 35 percent) at 6 GHz.

The first step of GaAs FET oscillator fabrication is to form an active subnetwork. This subnetwork consists of a feedback network from drain to gate on a 5-mm wide chip carrier [6]. The feedback network has a series connection of microstriplines on the alumina substrate and a chip capacitor of $BaO$–$TiO_2$ system ceramic plate metallized on both sides. An integrated GaAs FET oscillator is obtained by connecting an open-ended microstripline at the active subnetwork gate terminal and an output matching network at the drain terminal.

By optimizing the external feedback network, the FET chip can generate the maximum available output power. The unstabilized FET oscillator microwave performance is shown in Fig. 1 as a function of drain bias voltage $V_{DS}$ with gate bias voltage $V_{GS}$ fixed at $-3.8$ V. For 8 V $V_{DS}$ and $-3.8$ V $V_{GS}$, this oscillator generated 400-mW output power at 6000 MHz. The generated power level was comparable to the maximum added power of an amplifier using an FET chip obtained from the same wafer. The maximum dc to rf conversion efficiency of 38 percent was obtained at 7 V $V_{DS}$.

Oscillation frequency was sensitive to the gate bias voltage with a pushing figure around 200 MHz/V. The oscillation frequency depended on the length of the open-ended microstripline connected to the gate terminal of the active subnetwork. Fine-frequency adjustment was available, even after the subnetwork was completed, by making use of these dependencies.

0018-9480/78/0300-0156$00.75 

## III. Dielectric Resonant Circuit

The dielectric material used for the resonator is low-loss ceramic NED-39 developed in the NEC Central Research Laboratories. It principally consists of $BaTi_4O_9$. The microwave characteristics of this dielectric material were determined by measuring the $TE_{011}$ resonance frequency for a cylindrical resonator short-circuited with metal plates on both sides. At 6 GHz, the relative dielectric constant $\varepsilon_r$ is 39.5 and the unloaded $Q$ value is 7000. In the room temperature range, the thermal expansion coefficient $1/\ell \cdot \Delta\ell/\Delta T$ is $+8.8$ ppm/°C and the dielectric constant temperature coefficient $1/\varepsilon_r \cdot \Delta\varepsilon_r/\Delta T$ is $-23.8$ ppm/°C. The temperature effects of these two coefficients offset each other and cause a small temperature coefficient for the resonant frequency. The resonant frequency temperature coefficient $1/f_r \cdot \Delta f_r/\Delta T$ of a resonator fabricated from such a material can be approximated as follows:

$$\frac{1}{f_r}\cdot\frac{\Delta f_r}{\Delta T} \simeq -\frac{1}{2}\frac{1}{\varepsilon_r}\cdot\frac{\Delta\varepsilon_r}{\Delta T} - \frac{1}{\ell}\cdot\frac{\Delta\ell}{\Delta T}. \tag{1}$$

If the above-mentioned numerical values are substituted, the right-hand side of the equation equals $+3.1$ ppm/°C.

A simple theory was proposed by J. C. Sethares *et al.* [7] to determine the relationship between the resonator shape and resonant frequency. According to this theory the resonant frequency is given as a function of the relative dielectric constant $\varepsilon_r$, diameter $D$, and height $L$ of the cylindrical resonator.

$$L = \frac{\lambda_0}{\sqrt{\varepsilon_r - \left(\frac{x(mn)}{\pi}\cdot\frac{\lambda_0}{D}\right)^2}}\cdot\frac{1}{\pi} \cdot \arctan\frac{\sqrt{\left(\frac{x(mn)}{\pi}\cdot\frac{\lambda_0}{D}\right)^2 - 1}}{\sqrt{\varepsilon_r - \left(\frac{x(mn)}{\pi}\cdot\frac{\lambda_0}{D}\right)^2}}, \quad \lambda_0 = c/f_r \tag{2}$$

where $c$ is the light velocity in vacuum and $x(mn)$ is the $n$th zero of Bessel function $J_m(x)$. For the $TE_{01\delta}$ resonance mode, $x(01)$ equals 2.404.

In a practical resonant circuit, the dielectric resonator is placed on the alumina substrate and is confined within a metal case. The resonant circuit has a triple-layered structure of alumina substrate, cylindrical dielectric resonator and air gap, as is shown in Fig. 2. The resonant frequencies of such triple-layered structures are higher than the values evaluated by means of (2). In Fig. 3 resonant frequencies are shown as a function of resonator diameter $D$, while $L/D$ is fixed at 0.4 and alumina substrate thickness $\ell_2$ at 0.635 mm and 1.0 mm. In the figure, calculated resonant frequencies are also plotted as a reference. The resonant frequency $f_r$ decreases with increasing $D$ and $\ell_2$.

Fine adjustment of resonant frequency is possible by changing air gap thickness $\ell_1$ between the resonator and the metal disk. Fig. 4 shows a mechanical tuning characteristic of the resonant circuit containing a $D = 10$-mm and $L = 4$-mm resonator. By changing $\ell_1$ from 0 to 3.5 mm, mechanical tuning over 1000 MHz was obtained.

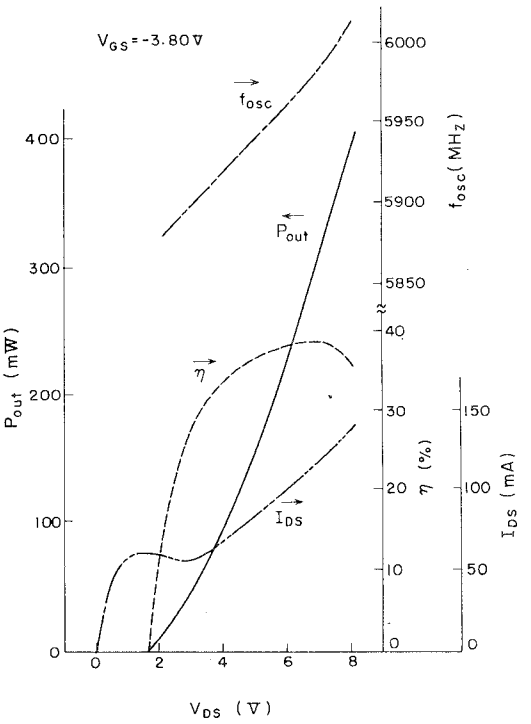


Fig. 1. Unstabilized oscillator microwave performance.

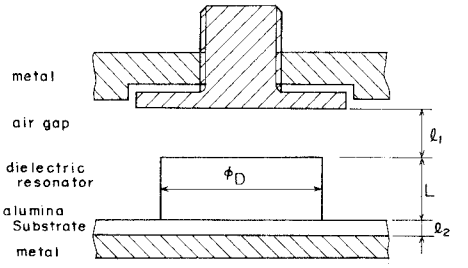


Fig. 2. Triple-layered structure of resonant circuit.

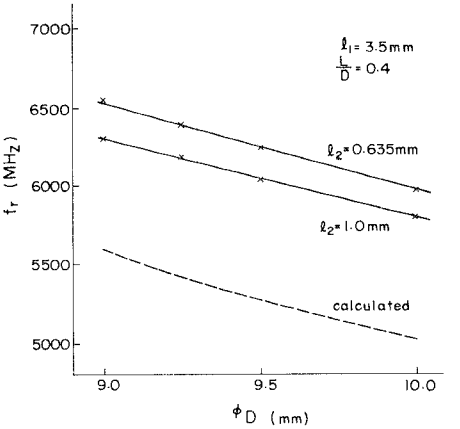


Fig. 3. Resonant frequency as a function of resonator dimension.

When a dielectric resonator is placed in the vicinity of a microstripline on the alumina substrate, magnetical coupling between resonator and line is caused. Coupling constant increases if distance $\ell_y$ between resonator edge and microstripline edge decreases. Reflection coefficients of the resonator of $D = 10$ mm and $L = 4$ mm, coupled to a 50-Ω

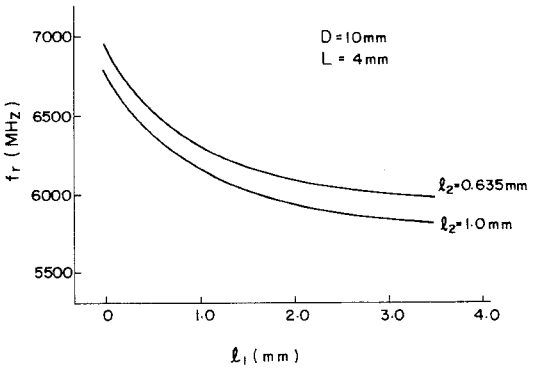


Fig. 4. Resonant frequency as a function of air gap thickness.

line terminated by a matched load, are shown in Fig. 5 for various distances, where the reference plane is placed $\lambda_g/2$ away from the resonator center position ($X_2 = \lambda_g/2$), where $\lambda_g$ is the microstrip wavelength. Distance $\ell_y$ is changed from 2.0 to 3.5 mm. It can be shown that the dielectric resonant circuit is expressed as a high-$Q$ parallel resonant circuit coupled to transmission line of characteristic impedance $Z_0 = 50\ \Omega$, as is shown in Fig. 6. By fitting the impedance locus in Fig. 5 to the following equation,

$$Z = Z_0\left(1 + \frac{\beta}{1 + 2 \cdot j \cdot Q_r \dfrac{\Delta f}{f_r}}\right), \quad \Delta f = f - f_r \qquad (3)$$

the coupling constant $\beta$ and the unloaded $Q$-value $Q_r$ for $\ell_y = 2.5$ mm were found to be 2.2 and 4000, respectively.

## IV. Coupling Between Oscillator and Resonant Circuit

A blockdiagram of a stabilized oscillator is shown in Fig. 7. The dielectric resonator is placed in the vicinity of a 50-Ω microstripline, which is connected to the drain output terminal of the active subnetwork, and constitutes a band rejection filter.

### *A. Load Characteristics of Unstabilized Oscillator*

Before coupling the unstabilized oscillator to the resonant circuit, large-signal impedances $Z_{osc}$ for the oscillator were measured. The Rieke diagram is shown in Fig. 8, where impedance $-Z_{osc}$ is plotted as the inverse of reflection coefficient $1/\Gamma_{osc}$.

$$1/\Gamma_{osc} = \frac{-Z_{osc} - Z_0}{-Z_{osc} + Z_0} \quad \text{Re}\ (Z_{osc}) < 0.$$

The reflection coefficient $\Gamma_{osc}$ is seen at the active subnetwork output terminal or at a plane located 2 mm away from the FET chip drain terminal. In a large-signal reflection coefficient measurement, a variable tuner was connected at the output terminal for adjusting power output or frequency and the reflection coefficient presented to the oscillator by the tuner were measured for constant power levels or constant frequencies. Under sustained oscillation conditions, the load reflection coefficient is equal to the inverse of the large-signal reflection coefficient of the unstabilized

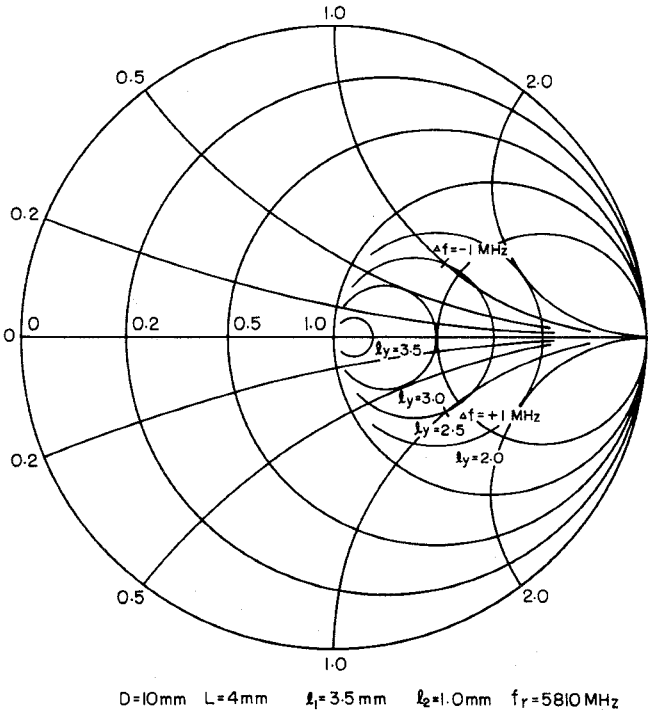


Fig. 5. Reflection coefficients of the resonator coupled to a terminated 50-Ω microstripline.

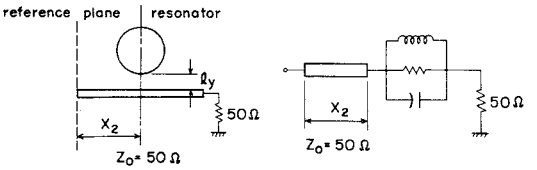


Fig. 6. Equivalent circuit of dielectric resonant circuit.

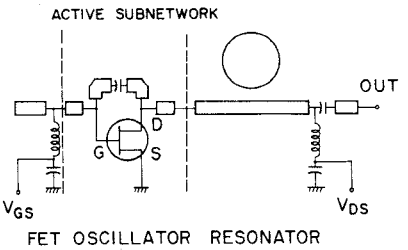


Fig. 7. Stabilized oscillator blockdiagram.

oscillator. From these contours of the unstabilized oscillator impedance, it was found that the oscillator is approximately expressed by a negative conductance, decreasing with increasing ac voltage, and $LC$ parallel resonant circuit, which terminate a 2-mm long line ($X_1 = 2$ mm, $2\pi X_1/\lambda_g \simeq \pi/5$), as is shown in Fig. 8.

From these RF properties of oscillator and resonant circuit, the optimum resonator center position was determined to be $\lambda_g/2$ away from the FET chip drain terminal, or ($\lambda_g/2 - 2$ mm) away from the active subnetwork output terminal. In Fig. 8 the impedance contour of the stabilizing band rejection filter is also plotted (dotted line). The operation point is marked with the letter $P$.

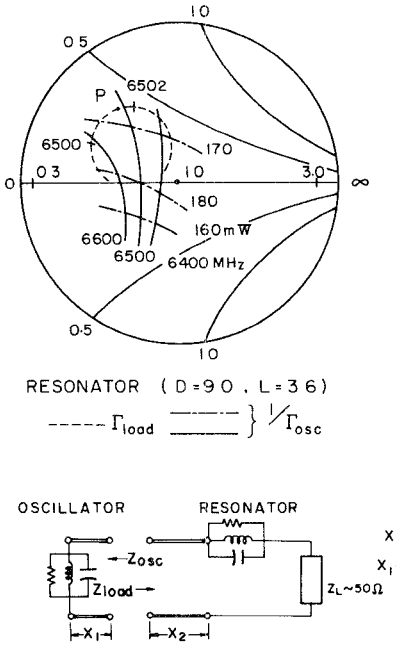


Fig. 8. Reflection coefficient $\Gamma_{osc}$ of unstabilized oscillator.

### B. Theoretical Aspect of Oscillator Stabilization

Stabilization of a solid-state microwave oscillator by loading a band rejection filter was theoretically investigated by K. Shirahata [8].

When a resonant circuit is placed at a point $n\lambda_g/2$ away from the negative conductance and is coupled to a transmission line terminated by a load with reflection coefficient $|\Gamma|e^{j\delta}$, oscillation frequency $f$ is obtained by equating total susceptance $B_t$ to zero under the condition, $\partial B_t/\partial f > 0$.

$$B_t = 2Q_0\left(\frac{f-f_r}{f_r}+\frac{f_r-f_0}{f_r}\right)\frac{f_r}{f_0}+\frac{2\beta Q_r\dfrac{f-f_r}{f_r}-b\left(1+4Q_r^2\left(\dfrac{f-f_r}{f_r}\right)^2\right)}{\left(1+\beta+a-2bQ_r\dfrac{f-f_r}{f_r}\right)^2+\left(b+2Q_r(1+a)\dfrac{f-f_r}{f_r}\right)^2}=0$$

$$a+jb=\frac{1+|\Gamma|e^{j\delta}}{1-|\Gamma|e^{j\delta}}-1\simeq 2|\Gamma|e^{j\delta} \tag{4}$$

where

$f_0$ unstabilized oscillator oscillation frequency,
$Q_0$ unstabilized oscillator external $Q$ value,
$f_r$ resonant circuit resonant frequency,
$Q_r$ resonant circuit $Q$ value,
$\beta$ coupling constant between resonant circuit and transmission line.

In the first term of the equation, $f_r/f_0$ is approximated as unity.

When the transmission line is terminated with a nonreflecting load, (4) can be converted to (5).

$$\frac{f_0-f_r}{f_r}=F\left(\frac{f-f_r}{f_r}\right)=\frac{f-f_r}{f_r}\cdot\left(1+\frac{\beta}{(1+\beta)^2}\cdot\frac{Q_r}{Q_0}\cdot\frac{1}{1+\left(\dfrac{2Q_r}{1+\beta}\cdot\dfrac{f-f_r}{f_r}\right)^2}\right). \tag{5}$$

By differentiating both sides of (5), derivatives $(\partial f/\partial f_0)_{f_r}$ and $(\partial f/\partial f_r)_{f_0}$ are obtained.

$$\left(\frac{\partial f}{\partial f_0}\right)_{f_r}=1/F^{(1)}\left(\frac{f-f_r}{f_r}\right)$$

$$\left(\frac{\partial f}{\partial f_r}\right)_{f_0}=\left(f-f_0/F^{(1)}\left(\frac{f-f_r}{f_r}\right)\right)\Big/f_r. \tag{6}$$

Four values of $f_0, f_r+f_a, f_r+f_b, f_r-f_b$, and $f_r-f_a (f_a>f_b)$, which make $(\partial f/\partial f_0)_{f_r}$ infinite, are obtained by solving (7).

$$F^{(1)}\left(\frac{f-f_r}{f_r}\right)=0 \tag{7}$$

and substituting the roots into (5). For $f_r-f_a<f_0<f_r-f_b$ and $f_r+f_b<f_0<f_r+f_a$, three values for $f$ which satisfy (5) exist but only the largest and the smallest ones satisfy the stable operating condition $\partial B_t/\partial f>0$. This brings about hysteresis in $f$ versus $f_0$ and $f$ versus $f_r$ relationships. Stabilization range $\Delta_a$, which includes hysteresis, and $\Delta_b$ which does not include hysteresis, are obtained by (8).

$$\Delta_a=2f_a$$

$$\Delta_b=2f_b. \tag{8}$$

Thanks to the unequality $Q_0 \ll Q_r$, $\Delta_a$ and $\Delta_b$ can be approximated as in (9).

$$\Delta_a\simeq\frac{1}{2Q_0}\cdot\frac{\beta}{1+\beta}f_r$$

$$\Delta_b\simeq 2\sqrt{\frac{\beta}{Q_0Q_r}}\cdot f_r. \tag{9}$$

Stabilized oscillator temperature coefficient $p$ and pushing figure $q$ are evaluated by means of (6).

$$p=\frac{1}{f}\frac{\Delta f}{\Delta T}=\frac{1}{f}\left[\left(\frac{\partial f}{\partial f_r}\right)_{f_0}\cdot\frac{\Delta f_r}{\Delta T}+\left(\frac{\partial f}{\partial f_0}\right)_{f_r}\cdot\frac{\Delta f_0}{\Delta T}\right]$$

$$q=\frac{\Delta f}{\Delta V_{GS}}=\left(\frac{\partial f}{\partial f_0}\right)_{f_r}\cdot\frac{\Delta f_0}{\Delta V_{GS}} \tag{10}$$

where $f=f_r=f_0$, $p$ and $q$ are expressed as functions of $f_r, Q_0$, $Q_r$, and $\beta$.

$$p=\frac{1}{f_r}\cdot\frac{\Delta f_r}{\Delta T}+\frac{1}{1+\dfrac{\beta}{(1+\beta)^2}\dfrac{Q_r}{Q_0}}\cdot\frac{1}{f_0}\cdot\frac{\Delta f_0}{\Delta T}$$

$$q=\frac{1}{1+\dfrac{\beta}{(1+\beta)^2}\dfrac{Q_r}{Q_0}}\cdot\frac{\Delta f_r}{\Delta V_{GS}}. \tag{11}$$

Pulling characteristics, when $f_0 = f_r$, are obtained by approximately solving (5), on the assumption that $|\Gamma| \ll \beta$, $|\Gamma| \ll 1$.

$$\frac{f - f_r}{f_r} \simeq \frac{b}{2Q_r\beta} \simeq \frac{|\Gamma|}{Q_r\beta}\sin\delta. \tag{12}$$

Maximum frequency deviation $(\Delta f)_{\text{pull}}$ is equal to $|\Gamma| \cdot f_r/(Q_r\beta)$. Where $f = f_0 = f_r$ and $|\Gamma| = 0$, load conductance seen at negative conductance is $Y_0/(1+\beta)$, where $Y_0$ is the transmission line characteristic admittance. As the output power level of the unstabilized oscillator changes with load conductance and band rejection filter insertion causes insertion loss, microwave power $P_L$ delivered to load $Y_0$ is reduced from that without band rejection filter.

$$P_L = P_0(Y_0/(1+\beta))/(1+\beta) = kP_0(Y_0)$$
$$k = \frac{1}{1+\beta}\cdot\frac{P_0(Y_0/(1+\beta))}{P_0(Y_0)} \tag{13}$$

where $P_0(G_L)$ is an unstabilized oscillator output power level, depending on load conductance $G_L$.

For designing a stabilized FET oscillator, frequency temperature coefficient, pushing figure, pulling characteristic, stabilization range width, and output power level have to be taken into account. These performances depend strongly on $\beta$. In the oscillator stabilization by a dielectric resonator, $\beta$ can be adjusted continuously by changing the resonator position. In this study, $\beta$ is selected to be around unity. The distance $\ell_y$ between resonator and line has to be selected with great care.

As a numerical example, the following values are substituted into (9)–(13):

$Q_0$ = 10,
$Q_r$ = 4000,
$\beta$ = 1,
$f_r$ = 6000 MHz,
$\frac{1}{f_0}\cdot\frac{\Delta f_0}{\Delta T}$ = −100 ppm/°C,
$\frac{1}{f_r}\cdot\frac{\Delta f_r}{\Delta T}$ = +3.1 ppm/°C,
$\left|\frac{\Delta f}{\Delta V_{GS}}\right|$ = 200 MHz/V,
$|\Gamma|$ = 0.13,
$P_0(Y_0/2)/P_0(Y_0)$ = 0.7.

Then

$\Delta_a$ = 150 MHz,
$\Delta_b$ = 60 MHz,
$p$ = +2.1 ppm/°C,
$q$ = 2 MHz/V,
$(\Delta f)_{\text{pull}}$ = 195 kHz,
$k$ = 0.35.

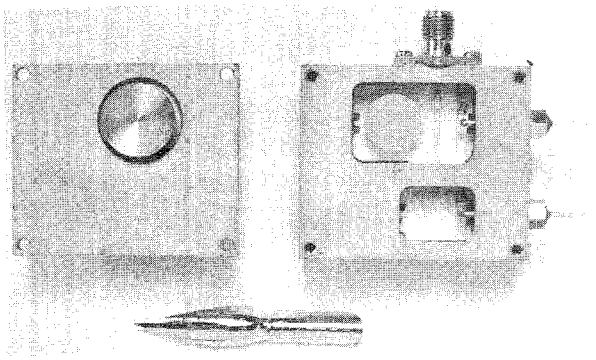

Fig. 9. Stabilized oscillator photograph. Right: top view of stabilized oscillator with a dielectric resonator. Left: case lid with metal disk.

## V. Stabilized Oscillator Structure

A complete stabilized oscillator photograph is shown in Fig. 9. The oscillator circuit is contained within a metal case. In the photograph the case lid is disassembled and is placed nearby. The circuit was formed on 1-mm or 0.635-mm thick alumina substrates. The active subnetwork, which contained FET chip and external feedback network, was placed on the base of the case under the metal wall. Open-ended microstripline at the gate terminal and 50-Ω microstripline at the drain output terminal were connected to dc bias circuits, which consisted of $\lambda_g/4$ high-impedance line and a chip capacitor. A chip capacitor was also used for cutting dc current off from output SMA connector. As shown in the photograph, the dielectric resonator was confined within a conductive wall to prevent spurious coupling with the feedback network or the open-ended line. A metal disk was attached to the case lid. It moved up and down with a sliding screw to change the air gap thickness between the resonator and the disk when the lid was assembled with the case.

## VI. Stabilized FET Oscillator Microwave Performance

Figs. 10–14 show the microwave performance of the frequency-stabilized GaAs FET oscillator with a dielectric resonator. Diameter $D$ and height $L$ of the cylindrical resonator are 10 mm and 4 mm, respectively. The alumina substrate thickness is 1 mm for Figs. 10 and 11 and 0.635 mm for Figs. 12–14.

Fig. 10 shows oscillation frequency $f_{\text{osc}}$ and output power level $P_{\text{out}}$ dependences on gate bias voltage $V_{GS}$, while ambient temperature $T_a$ and drain bias voltage $V_{DS}$ are fixed. Oscillation frequency was stabilized over the gate bias range of −3.1 to −4.3 V. The pushing figure was about 3 MHz/V. Hysteresis curves were observed on both sides of the stabilized range. Hysteresis phenomena were also observed in $V_{GS}$ dependence of drain bias current $I_{DS}$. An abrupt jump of $I_{DS}$ from 135 to 87 mA, observed at $V_{GS}$ of −3.08 V with the frequency jump from 5690 to 5810 MHz, suggests a sudden operation point shift.

Fig. 11 shows $f_{\text{osc}}$ and $P_{\text{out}}$ deviations for the ambient temperature range from 0 to 50°C. $V_{DS}$ and $V_{GS}$ were fixed at 7.0 V and at −3.2 V. The positive temperature coefficient for resonant frequency compensated for the negative tempera-

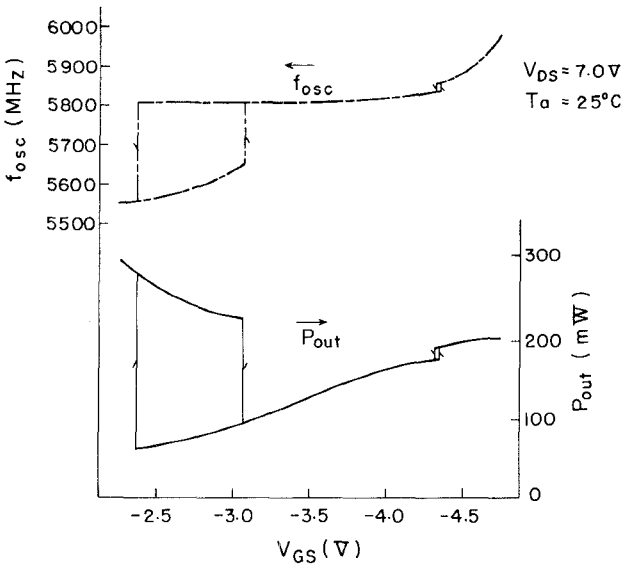


Fig. 10. Stabilized oscillator microwave performance as functions of gate-source bias voltage $V_{GS}$.

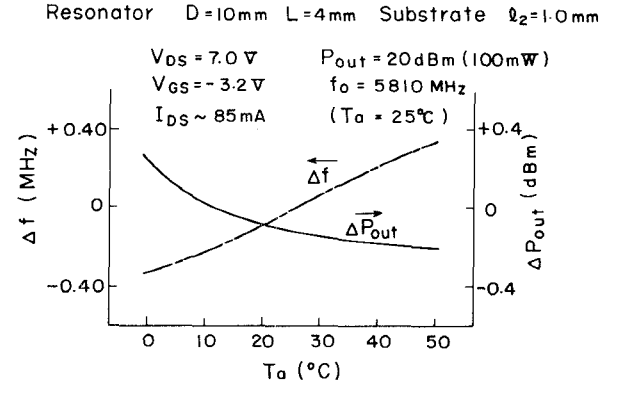


Fig. 11. Deviations in $P_{out}$ and $f_{osc}$ for ambient temperatures between 0 and 50°C.

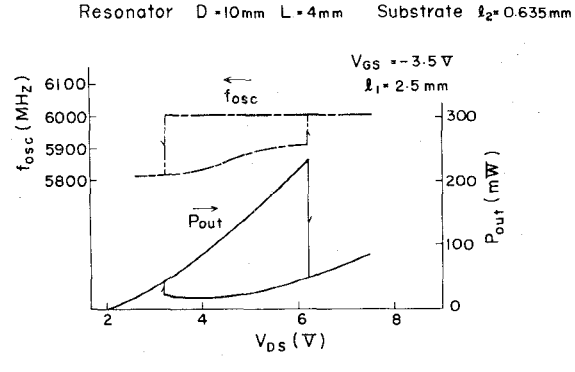


Fig. 12. Stabilized oscillator microwave performance as functions of drain-source bias voltage $V_{DS}$.

ture coefficient of unstabilized oscillator and brought about a small frequency temperature coefficient as low as +2.3 ppm/°C. Deviations in $f_{osc}$, $P_{out}$, and $I_{DS}$ are ±0.34 MHz, ±0.2 dBm, and ±3 mA, respectively. At 25°C ambient temperature $T_a$, $f_{osc}$, $P_{out}$, $\eta$, and $I_{DS}$ are 5810 MHz, 20 dBm (100 mW), 17 percent, and 85 mA, respectively.

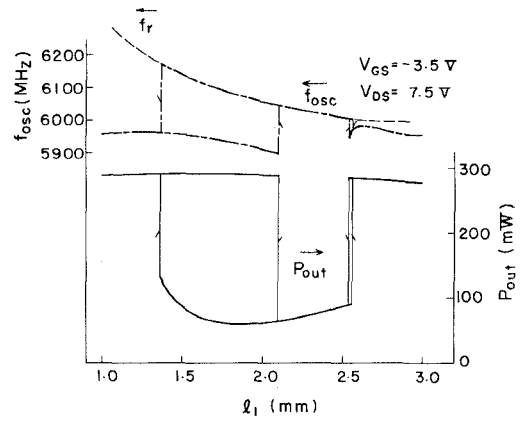


Fig. 13. Mechanical tuning characteristics of stabilized oscillator.

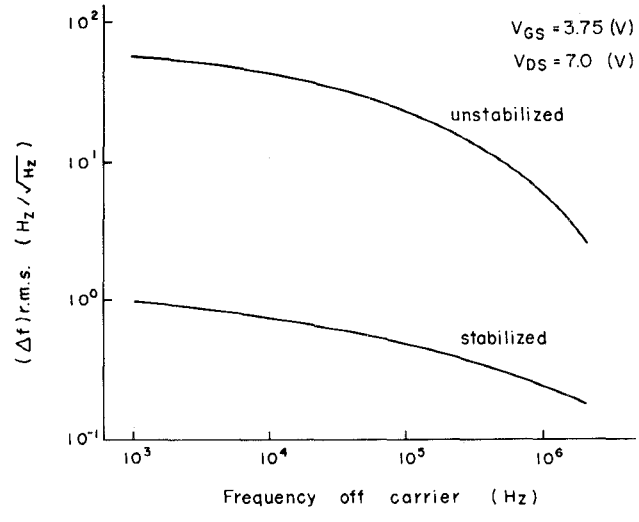


Fig. 14. FM noise characteristics of unstabilized and stabilized oscillators.

Fig. 12 shows $V_{DS}$ dependences of $f_{osc}$ and $P_{out}$, while the gate was biased at −3.5 V. The oscillator was always pulled into the stabilized state as long as $V_{DS}$ was greater than 6.5 V.

To show the mechanical tuning characteristic of the stabilized oscillator, $f_{osc}$ and $f_r$ are plotted as functions of air gap thickness $\ell_1$ in Fig. 13. Air gap thickness $\ell_1$ in the resonant circuit triple-layered structure was changed by moving the metal disk with a sliding screw. If $\ell_1$ is restricted within the range between 2.1 and 2.6 mm, $f_{osc}$ follows resonant frequency without showing any hysteresis characteristic from 6000 to 6050 MHz.

FM noise characteristics were also markedly improved by introducing a dielectric resonator. $(\Delta f)_{rms}$ in the 1-Hz band was 0.4 $Hz/\sqrt{Hz}$ at 200-kHz off carrier and exhibited a noise reduction of more than 30 dB from that of the unstabilized oscillator (Fig. 14). The external $Q$ value was about 2000.

Frequency stability and stabilization range for the obtained stabilized oscillator show a reasonable agreement with the numerical values presented in Section IV. This demonstrates an excellent designability of the stabilized oscillator with a dielectric resonator. Part of the discrepancy between theory and experiment is attributable to the neglected ac voltage dependence of oscillator susceptance.

## VII. Conclusion

Design theory, fabrication procedure, and performance of a highly stabilized GaAs FET oscillator with a high-$Q$ dielectric resonator have been described. A newly developed low-loss dielectric material with a small frequency temperature coefficient as low as 3.1 ppm/°C was successfully applied to stabilizing a high-power high-efficiency GaAs FET oscillator.

The compact stabilized oscillator exhibited a 100-mW output power level with 17-percent efficiency and a frequency temperature coefficient as low as +2.3 ppm/°C. FM noise level was improved more than 30 dB by stabilization. These performances will be sufficient to be applied to microwave communication systems.

## Acknowledgment

The authors wish to express their sincere gratitude to S. Aihara for his cooperation in FM noise measurement; T. Sugiura for helpful discussions and K. Ayaki, T. Okada, H. Katoh, and F. Hasegawa for their constant encouragement through this study.

## References

[1] H. Abe, Y. Takayama, A Higashisaka, R. Yamamoto, and M. Takeuchi, "A high-power microwave GaAs FET oscillator," *IEEE Int. Solid-State Circuits Conf. Digest of Tech. Papers*, pp 164–165, Feb. 1976.

[2] D. S. James, G. R. Painchaud, E. Minkus, and W. J. R. Hoefer, "Stabilized 12 GHz MIC oscillators using GaAs FET's," in *Proc. 5th European Microwave Conf.*, pp. 296–300, Sept. 1975.

[3] T. L. Heyboer and F. E. Emery, "YIG-tuned GaAs FET oscillators," in *Proc. IEEE/GMTT Inter. Microwave Symp.*, pp. 48–50, June 1976

[4] G. Satoh, "Stabilized microstrip oscillator using a temperature-stable dielectric resonator," in *IEEE Int. Solid-State Circuits Conf. Digest of Tech. Papers*, pp. 184–185, Feb. 1974.

[5] A. Higashisaka, R. Yamamoto, Y. Takayama, and M. Takeuchi, "Microwave medium-power GaAs SBFET," National Convention of IECE, Japan, S3-4, Apr. 1976.

[6] H. Abe and Y. Takayama, "A high-power microwave GaAs FET oscillator," in *NEC Research and Development*, Apr. 1977.

[7] J. C Sethares and S. J. Naumann, "Design of Microwave Dielectric Resonators," *IEEE Trans. Microwave Theory Tech.*, vol. MTT-14, pp. 2–7, Jan. 1966.

[8] K. Shirahata, "Stabilization of solid state microwave oscillator by loading BRF," presented at 1969 European Microwave Conf (London), Sept 1969.

# Dynamic Considerations of Injection Locked Pulsed Oscillators with Very Fast Switching Characteristics

DIMITRIOS PAVLIDIS, HANS LUDWIG HARTNAGEL, AND KAZUTAKA TOMIZAWA

***Abstract*—A theory is reported which describes, in a more accurate manner than previously, the voltage and phase transients of injection locked pulsed oscillators with very fast growth times by incorporating second-order effects which become important under certain conditions. The locking transients are determined either in the time domain or on a phase plane in which the variables are the oscillation amplitude and the phase $\phi$. The optimum conditions for fast switching are demonstrated with the aid of experimentally obtained data for Gunn oscillators, which give some experimental verification of the theory presented here.**

Manuscript received December 17, 1976; revised June 27, 1977.

D. Pavlidis was with the Department of Electrical and Electronic Engineering, University of Newcastle upon Tyne, NE1 7RU, England. He is now with the Institut fur Hochfrequenztechnik, Technische Hochschule Darmstadt, Darmstadt 6100, Germany.

H. L. Hartnagel is with the Department of Electrical and Electronic Engineering, University of Newcastle upon Tyne, NE1 7RU, England.

K. Tomizawa is with the Faculty of Engineering, Meiji University, 5158 Ikuta, Tama-Ku, Kawasaki, Japan.

## I. Introduction

THE SYNCHRONIZATION of negative resistance oscillators has been the subject of theoretical and experimental treatments. The study of the steady state synchronization properties was pioneered by Van der Pol [1]. A better physical understanding together with a transient analysis for the case of low-level injected signals has been provided by Adler [2]. The case of strong driving signals has been considered by Paciorec [3], while Huntoon and Weiss [4] refined Adler's theory, predicting the potential future of the synchronization phenomena in the development of oscillators suitable for microwave applications. The most outstanding, recent work has been contributed by Kurokawa [5], [6], whose analysis, however, neglects second-order effects. Many applications aim at fast growth times of oscillations. By way of example of such an applica-

0018-9480/78/0300-0162$00.75 